# Characterizations of the Non-linear Responses of a Non-premixed Flame to the Low Frequency Acoustic Excitations

Deng Pan , Chenzhen Ji , Tong Zhu *

Posted Date: 26 April 2023

doi: 10.20944/preprints202304.0962.v1

Keywords: non-premixed flame; flame describing function; nonlinear response; bluff-body; convective velocity

*Article*

# Characterizations of the Non-Linear Responses of a Non-Premixed Flame to the Low Frequency Acoustic Excitations

**Deng Pan, Chenzhen Ji and Tong Zhu ***

School of Mechanical and Engineering, Tongji University, Shanghai, 201804, China
* Correspondence: zhu_tong@tongji.edu.cn

**Featured Application: Stable design of Combustor in industrial boiler and burner**

**Abstract:** The heat release response of the flame to acoustic excitation is a critical factor for understanding combustion instability. In the present work, the nonlinear heat release response of a methane-air non-premixed flame to the low frequency acoustic excitations is experimentally investigated. The flame describing function (FDF) was measured based on the overall CH* chemiluminescence intensity and the velocity fluctuations obtained by two-microphone method. The CH* chemiluminescence images and the schlieren images were analyzed to reveal the mechanism of nonlinear response. The excitation frequency ranges from 10Hz to 120Hz. The forced relative velocity fluctuation amplitude ranges from 0.10 to 0.50. The corresponding flame Strouhal number ($St_f$) ranges from 0.43 to 4.67. The study has shown that the flame length responds more sensitively to changes in excitation amplitude when subjected to relatively high frequency excitations. The normalized flame length ($L_f/D$) decreases from 3.79 to 2.37 with the increase of excitation amplitude at excitation frequency of 100Hz. The number of oscillation zones along the flame increases with increasing excitation frequency, which is consistent with the increase of the $St_f$. The low-pass filtering characteristic of FDF is caused by the dispersion of multiple oscillation zones, as well as the cancellation effect of the adjacent oscillation zones under relatively high frequency excitation. The cancellation effect of the positive and negative oscillation zones with various $St_f$ is main mechanism for the local gain peak and valley. When two adjacent oscillation regions have approximate amplitudes, the overall phase-lag becomes more sensitive to changes in excitation frequency and amplitude. This sensitivity leads to nonlinear anomalous changes in the phase-lag near the frequency corresponding to the gain valley. The calculated disturbance convection time is consistent with the measured time delay in the short flame scenario. Future research is necessary to establish whether the observed agreement occurs due to the oscillation zone consistently occurring proximate to the flame's center of mass, coupled with a precise determination of the average convective velocity.

**Keywords:** non-premixed flame; flame describing function; nonlinear response; bluff-body; convective velocity

## 1. Introduction

Combustion instability has been an issue in the low NOx emission combustion equipment. It is manifested as large amplitude fluctuations of pressure and heat release in combustion chamber, which may lead to structural damage. This instability is attributed to the interaction of the unsteady heat release and the cavity acoustic modes of the combustion chamber [1]. Therefore, the response characteristic of heat release rate (HRR) to the flow perturbations is a key role to better understand the combustion instability [2–4]. Previous studies have established related models to describe the response of the heat release to the flow disturbance. Among them, the n-τ model and the flame transfer function (FTF) were based on the linearization assumption [5,6]. The frequency and the corresponding growth rate of the thermoacoustic oscillations can be predicted through the combination of the linear flame response models and the thermoacoustic coupling model [7]. However, the linear FTF cannot interpret the nonlinear thermoacoustic features, such as the mode

switching, nonlinear triggering and frequency shifting [8], as well as obtaining the oscillation amplitude in limit cycle mode. Therefore, in order to determine the nonlinear response of the flame, the flame describing function (FDF) was proposed [9]. The FDF considers the effects of the forcing amplitude in addition to the frequency. Noiray et. [10] used FDF of a premixed flame to interpret the mode switching phenomenon and predict the limit cycle amplitudes of oscillation. The theoretical results were in excellent agreement with measurements. FTF and FDF can be obtained through CFD numerical simulation and theoretical analysis and experiments [5,11,12]. With the experiment, the HRR response can be measured by optical equipment, such as the PMT, OH-PLIF, or the ICCD camera integrated with CH* or OH* chemiluminescence filter [13,14].

Much work has been reported related to the responses of the premixed flame with different configurations, such as, laminar conical flames [15,16], multiple conical flames [17], swirled flames [18–20], bluff-body stabilization flames [21] and practical gas turbine burner [22–24]. Compared to the premixed flame, there are relatively few studies on the response characteristics of non-premixed combustion. Existing works mainly focused on the laminar jet diffusion flame. In order to understand the foundational mechanism, a lot of literatures have worked on the forced response of the Burk-Schumann diffusion flame with theoretical analysis. Tyagi et al. [25] theoretically studied the heat release of the Burke-Schumann flame to the longitudinal velocity fluctuations with the assumption of the uniform flow field. It was found that the Da number plays an important role in determining the amplitude and phase of the heat release fluctuations with respect to the velocity fluctuations. Based on the same flame and assumptions, Chandrasekhar and Chakravarthy [26] investigated the response of the flame to transverse velocity oscillations. The gain of heat release response was nearly independent of the amplitude at low frequencies. However, the gain decreased with the increase in the excitation amplitude. Nicholas et al. [27,28] compared the dynamics of the forced response of laminar non-premixed and premixed flames to the velocity fluctuations. Mass burning rate oscillations dominate the response of non-premixed jet flame, however, the perturbations of the flame speed and the burning area induced by the velocity fluctuations caused the oscillations of the HRR for the premixed flame [29]. Corresponding to the different response mechanisms, the gain and phase-lag of the FTF of the jet diffusion flame and premixed flame were also much different, especially under low flame Strouhal number ($St_f$). Yao and Zhu [30] discussed the distributed FTF for the Burke-Schumann diffusion flame with Green's Function method. A dual-peak amplitude of the gain was observed in the fuel-rich zone and the fuel-lean zone respectively. The effects of the Strouhal number, the Peclet number and convective on hot spot propagation were also discussed, which were related to the entropy wave.

Some experimental works were also conducted to obtain the HRR response of the jet diffusion flame. Jiang et al. [31] studied the forced reacting plumes of a jet non-premixed flames and discussed the interaction of the buoyancy-driven instability and the convective instability. The flame pinch off was observed with the strong low frequency perturbations and the flame exhibits a low-pass filter characteristic. The dynamics of the jet diffusion flame in a standing wave have been studied [32–36]. The low-pass characteristic of the response of the jet diffusion flame have also been observed in this geometry. The effects of the excitation frequency and amplitude, the position of the fuel nozzle and the fuel type on the flame dynamics were discussed in these papers. Kim et al. [37] measured the FDF of a coaxial jet diffusion flame with the excitation frequency of 80Hz to 200Hz. The gain of the FDF was independent of the forced amplitude. However, the phase-lag of the FDF has a trend of decreasing with the forced amplitude.

In the past researches, the non-premixed flame was usually treated as an active control method of combustion instability in premixed flame. However, in recent studies, the self-excited combustion instability of non-premixed flame have also been observed and discussed [38,39]. For the industrial burner the air and fuel were usually organized in cross-flow jet for the objective of enhancing mixing process. In order to anchor the flame, the bluff-body was used as the flame stabilization structure. The stabilization mechanism of such bluff-body non-premixed flames has been studied [40]. Hardalupas and Selbach [41] investigated the effect of the excitation frequency and the amplitude on the flame lift-off height and the reattachment, as well as the combustion efficiency and emissions of

Preprints (www.preprints.org) | NOT PEER-REVIEWED | Posted: 26 April 2023 doi:10.20944/preprints202304.0962.v1



a radial injector non-premixed flame. However, the heat release response characteristics to the acoustic excitation are not clearly studied.

Another factor affecting combustion stability is the acoustics characteristics of the combustion chamber cavity, which is mainly determined by its geometry dimensions and the flow field parameters. The natural oscillation mode is presented as a low frequency in practical industrial combustion equipment determined by the geometry parameters of the large cavity [42,43]. Therefore, its response to low frequency excitation is noteworthy.

In summary, many attempts have been made to understand the response mechanism of the non-premixed flame with different geometries. However, much less data is available for systematic studies of the FTF and FDF of the non-premixed flame to the acoustic perturbations, especially in experiments. The effects of the excitation frequency and amplitude on the phase-lag and gain of the FTF and FDF of the non-premixed flame are not yet clear.

The objective of present work aims to investigate the characteristics of the response of a methane-air bluff-body non-premixed flame to low-frequency forced acoustic excitation on the air flow. The FDF of the flame was measured. The spatial heat release response of the flame was analyzed with the CH* chemiluminescence images and schlieren images. The research results aim to broaden the scope of the mechanism of the interaction of the forced flow perturbations and unsteady combustion, and provide foundation for the prediction of combustion instability of the non-premixed flame. The results may provide instructions for the design of stable combustion in industrial burners.

## 2. Experimental Setup and Measurements

The experimental setup consisted of a bluff body diffusion burner equipped with an acoustic forcing system, and diagnostics for flow, acoustic and flame dynamics as shown in **Figure 1**. The burner was designed with a plate bluff-body and four radial methane nozzles with a diameter of 3mm. The bottom of the test rig was fitted with a loudspeaker cavity, housing a 140mm diameter speaker that was powered by a power amplifier (YAMAHA, PX8). The acoustic signal was modulated by a RIGOL DG1022z signal generator, which controlled the frequency of the sin-wave signal. Both the power amplifier and the signal generator modulated the amplitude of the forced power. The air supply was provided by an air compressor.

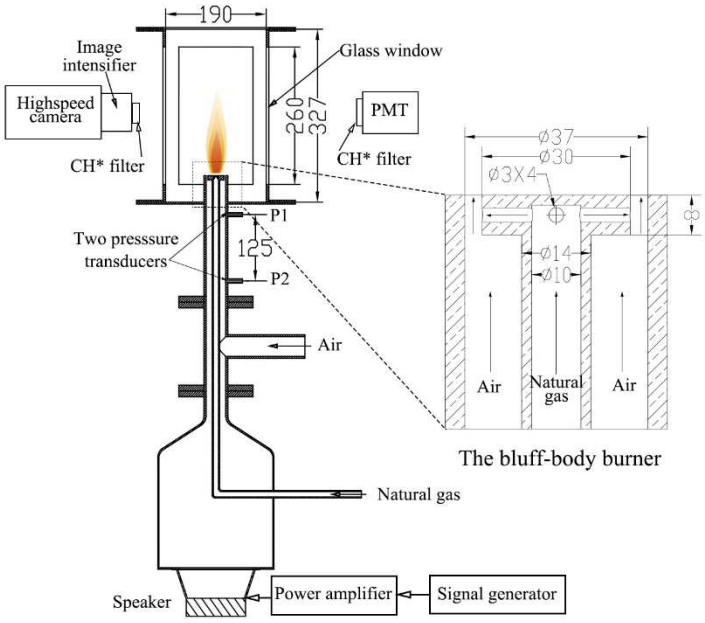


**Figure 1.** Schematic of the experimental setup. Unit: mm.

A Thorlabs PMM01 photomultiplier tube (PMT) equipped with a narrow bandpass filter (Thorlabs FB430-10) at a wavelength of 430nm±10nm was used to monitor the overall flame CH* chemiluminescence release, with the PMT signal proportional to the heat release. Two GRAS 46BE

Preprints (www.preprints.org) | NOT PEER-REVIEWED | Posted: 26 April 2023 doi:10.20944/preprints202304.0962.v1



flush-mounted microphones were installed at the burner inlet to calculate the velocity fluctuation amplitude and phase using the two-microphone method [44], based on the collected signals from the two microphones. The distance between the two microphones was 125mm. Balachandran et al. [45] reported good agreement between the excited velocity fluctuation amplitude and phase measured by the hot wire and two-microphone method in the frequency range of 20~500Hz.

The PMT and microphone signals were simultaneously recorded at a frequency of 5kHz using a data acquisition system (NI-cDAQ-9174, NI9239, NI9234). A high-speed camera (HSC) (AgileDevice M220) integrated with an image intensifier (EyeiTS S-HQB-F) and a narrow bandpass filter at a wavelength of 430nm±10nm were employed to capture the CH radicals release of the flame at a sampling frequency of 2000fps, with an exposure time of 0.45ms for each image. The amplification factor of the image intensifier was set to the same value under different experimental conditions.

A Z-type schlieren photography system was established to observe the flame hot gas structure response. It consists of a pair of parabolic mirrors (250mm in diameters and 2.5m focal length), a point-light source, a knife edge and a high-speed camera (AgileDevice, M220). The schlieren time-resolved flame images were captured with a frame rate of 2000 fps, exposure time of 0.05ms and image size of 1080*1920 pixels. The schlieren system and the CH* chemiluminescence images were not synchronized, however the schlieren system was synchronized with microphone signal acquisition.

The methane used in the experiment was sourced from a natural gas pipeline, with a low heat value of 34.5 MJ/Nm$^3$ and a methane volume fraction of 94.4%. The natural gas flow rate was maintained at 0.42 Nm$^3$/h, while the air flow rate was set to 4.67 Nm$^3$/h, resulting in an overall equivalence ratio of 0.86, which represents the normal operating condition of an industrial boiler. The mean air velocity before the nozzle was $\bar{u}$=1.41 m/s, and the natural gas velocity at the gas nozzle was 4.14 m/s. The air jet flow velocity at the ring of the nozzle was $u_0$=3.52m/s. The velocity excitation frequency ranged from 10Hz to 120Hz, with an interval of 5Hz in the low frequency range of 10Hz to 50Hz, and an interval of 10Hz in the excitation frequency range of 50Hz to 100Hz. The relative velocity excitation amplitude ranged from 0.10 to 0.50. The operating conditions are shown in **Table 1**.

**Table 1.** The operating conditions for the burner and acoustic excitations.

| Parameters | Values |
|---|---|
| Gas flow rate (Nm$^3$/h) | 0.42 |
| Air flow rate (Nm$^3$/h) | 4.67 |
| Air velocity in the ring, $u_0$ (m/s) | 3.52 |
| Air velocity before the nozzle, $\bar{u}$ (m/s) | 1.40 |
| gas velocity at the nozzle, $u_{gas}$ (m/s) | 4.10 |
| Equivalence ratio | 0.86 |
| Excitation frequency, $f_e$ (Hz) | 10, 15, 20, 25, 30, 35, 45, 50, 60, 70, 80, 90, 100, 120 |
| Excitation amplitude, $u'/\bar{u}$ | 0.10, 0.20, 0.30, 0.40, 0.50 |

## 3 Data analysis Method

### *3.1 Flame Describing Function Model*

The flame transfer function (FTF) is defined as the ratio of the HRR fluctuation and the relative velocity fluctuation at the reference position of inlet of the burner:

$$FTF(f_e) = \frac{Q'/\bar{Q}}{u'/\bar{u}} = G(f_e)e^{-j\Delta\varphi(f_e)} \quad (1)$$

Where, $Q'/\bar{Q}$ is the HRR fluctuation, $u'/\bar{u}$ is the normalized velocity fluctuation at the reference position of inlet of the burner (P1). It can be written in frequency domain as a complex number with a gain $G$ and a phase-lag $\Delta\varphi$.

Preprints (www.preprints.org) | NOT PEER-REVIEWED | Posted: 26 April 2023 doi:10.20944/preprints202304.0962.v1



When the excitation amplitude of the relative velocity fluctuation is taken into consideration, the FTF can be extended to FDF, as Eq. (2).

$$FTF(|u'/\bar{u}|, f_e) = \frac{Q'/\bar{Q}}{u'/\bar{u}} = G(|u'/\bar{u}|, f_e)e^{-j\Delta\varphi(|u'/\bar{u}|, f_e)} \quad (2)$$

To obtain the FDF, the velocity fluctuations at the upstream of the burner were measured using the two-microphone method, while the overall HRR of the flame was measured using the PMT. The reference position for the velocity fluctuations was set at the pressure measuring point P1, which was located 73.5mm away from the top of the bluff-body. The analogue signals from the microphones and the PMT were measured simultaneously and transformed into the frequency domain using the fast Fourier transform (FFT). The HRR is derived from the PMT signal using Eq. (3):

$$\frac{Q'}{\bar{Q}} = \frac{I_{CH^*} - \overline{I_{CH^*}}}{\overline{I_{CH^*}}} \quad (3)$$

where, $I_{CH^*}$ represents the analogue signal obtained from the PMT, and $\overline{I_{CH^*}}$ represents the time-averaged analogue signal of the PMT over 1 second.

### *3.2 Flame Length and Height of Center of Mass of the Flame*

In order to evaluate the flame dynamics, two critical parameters of the flame are obtained based on the CH* chemiluminescence images: the flame length ($L_f$) and the center of mass of the flame ($P_{fy}$). The flame length is defined as the axial length of the flame which determined by the CH* chemiluminescence images whose pixel gray value (g) are larger than $0.1g_{max}$. $g_{max}$ is the maximum gray value for a flame CH* chemiluminescence image. The height of center of mass (COM) of the flame is defined as Eq. (4):

$$P_{fy} = \frac{\int g(x,y)ydy}{\int g(x,y)dy} \quad (4)$$

where $g(x,y)$ is the gray value of the image at position ($x$, $y$). The symbol "x" is used to indicate the horizontal dimension, whereas the symbol "y" represents the axial dimension. (x, y) is the actual coordinate of the flame corresponding to the image pixel.

Figure 2 displays the flame length and height of COM for a time-average image of the flame. The influence of the excitation frequency and amplitude on the two parameters will be discussed in *Section 4.2*.

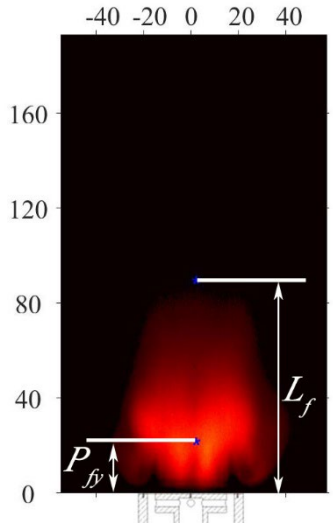


**Figure 1.** Schematic diagram of flame length and the height of COM

Preprints (www.preprints.org) | NOT PEER-REVIEWED | Posted: 26 April 2023 doi:10.20944/preprints202304.0962.v1



*3.3 Flame Strouhal Number*

The flame Strouhal number ($St_f$) is a critically normalized value used to analyze the characteristics of the flame's response to acoustic excitations [46]. The $St_f$ can be used to unify the gain of the FTF [47]. The $St_f$ refers to the number of perturbations induced by acoustic excitations along the flame. It relates the frequency of flame oscillations to the fluid dynamics that govern them. It defines as Eq. (5),

$$St_f = \frac{L_f f_e}{u_{cv}} \tag{5}$$

where $u_{cv}$ is the convective velocity of the excited flow perturbation along the flame. $f_e$ is the excitation frequency. $L_f$ is the flame length. Here, the mean convective velocity was defined as the jet velocity at the ring of the burner, $u_{cv}=u_0=3.52$m/s.

*3.4 Axial Distribution of Heat release Fluctuation*

In order to investigate the spatial distribution of heat release oscillations, horizontal integration was performed on images of CH* chemiluminescence, which reveal the characteristics of axial oscillation. The time-averaged axial distribution within one excitation cycle was then subtracted from the results to obtain the transient axial distribution of relative heat release fluctuations. It defined as Eq. (6),

$$I'(y,\tau) = \int g(x,y,\tau)\,dx - \int\int g(x,y,\tau)dxd\tau \tag{6}$$

where $I'(y,\tau)$ represents the transient axial distribution of relative heat release fluctuations, and $g(x,y,\tau)$ represents the pixel gray value of the CH* luminescence image corresponding to the actual position $(x,y)$.

**4. Results and Discussions**

*4.1 Measured Flame Describing Function*

Figure 3 shows the gain and phase-lag of the FDF under different excitation amplitudes obtained through PMT. The gain and phase-lag exhibit different frequency evolutions under different amplitudes of driving force. This indicates the nonlinear response of the flame. The gain exhibits a typical low-pass filter feature. When the frequency exceeds 80Hz, the gain consistently remains smaller than 0.25. The gain at $f_e$=10Hz is significantly larger than the gain at other frequencies. A local gain peak is observed near 30-35 Hz, and a local gain valley appears at 15-20 Hz under most excitation amplitudes. The saturation effects of the excitation amplitudes are not observed, and the gain increases trendily as the excitation amplitudes increase, especially for relatively higher frequencies of $f_e$=45-80Hz. The phase-lag evolution with frequency varies significantly under different excitation amplitudes, particularly when the frequency is below 25Hz. Specifically, at an excitation frequency of 20Hz, the phase-lag is close to $2\pi$ when the excitation amplitude is below 0.20. However, if the excitation amplitude is greater than 0.20, the phase-lag equals approximately $0.5\pi$. The overall trend of phase-lag variation with excitation frequency is almost linear when the excitation frequency exceeds 25Hz, with a slight dip near 50Hz, followed by an increase. Notably, the frequencies corresponding to the anomalous phase-lag change (15Hz-20Hz and 45Hz-50Hz) are close to the frequencies associated with the valleys of the gain. In previous studies [48,49], this anomalous variation of phase-lag, which corresponds to the frequency band where the gain valley occurs, has been observed. In the following sections, we will elucidate these non-linear phenomena by analyzing the dynamic changes in flames.

Preprints (www.preprints.org) | NOT PEER-REVIEWED | Posted: 26 April 2023 doi:10.20944/preprints202304.0962.v1



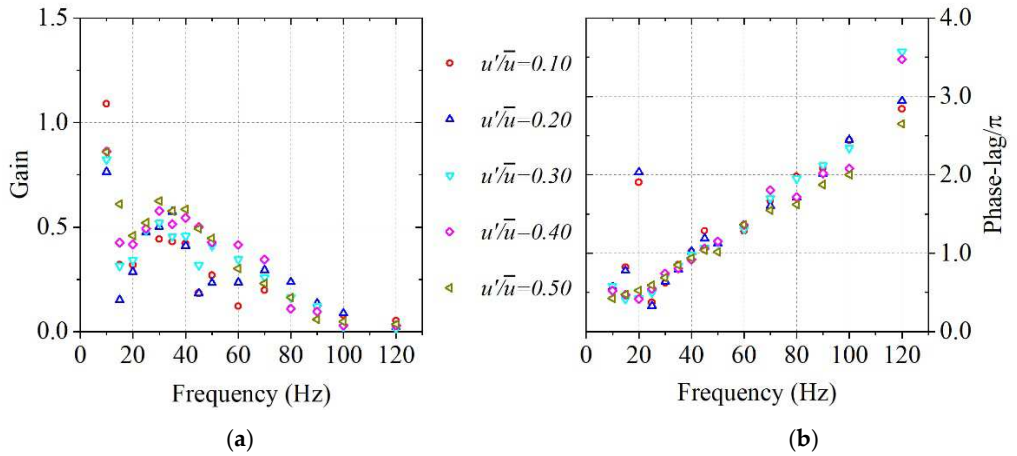


**Figure 2.** Measured flame describing function: (a) The evolution of the gain with excitation frequency at different excitation amplitudes; (b) The evolution of the phase-lag with excitation frequency at different excitation amplitudes.

*4.2 Time-Averaged Flame Response*

This section discusses the influence of excitation frequency and amplitude on the time-average distribution of the flame, which includes the flame length and the height of the COM. Figure 4 shows the time-average distribution of CH* chemiluminescence under different excitation conditions. The corresponding length of the flame ($L_f$) and height of the COM ($P_{fy}$) for different excitation frequencies and amplitudes is shown in Figure 5. The $L_f$ and the $P_{fy}$ are more sensitive to excitation amplitudes at relatively higher excitation frequencies. At frequencies of 10Hz-20Hz, $L_f$ appears to be independent of excitation amplitudes, but the main heat release zone is more uniform at higher excitation amplitudes. For relatively large frequencies (50Hz and 100Hz), $L_f$ shows a decreasing trend with increasing excitation amplitude, and it decreases as the frequency increases at the same excitation amplitude. The normalized flame length ($L_f$/D) decreases from 3.79 to 2.37 as the excitation amplitude increases from 0.10 to 0.50 at an excitation frequency of 100Hz. Here, D=0.037m represents the air channel diameter.

Preprints (www.preprints.org) | NOT PEER-REVIEWED | Posted: 26 April 2023 doi:10.20944/preprints202304.0962.v1



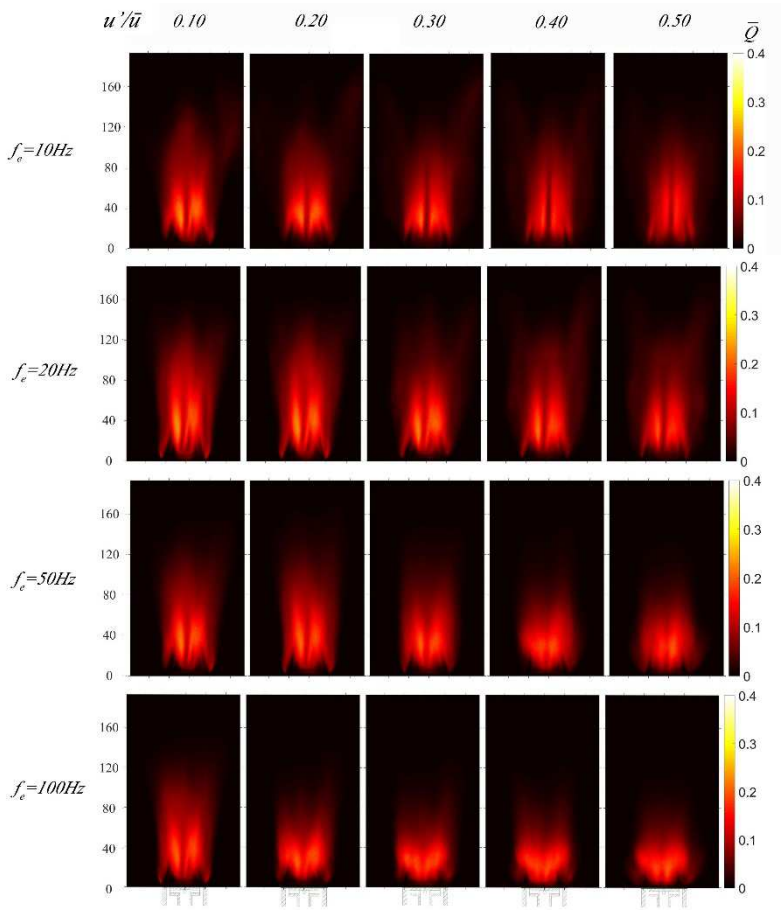


**Figure 3.** The time-averaged distributions of CH* chemiluminescence with different excitation frequencies and amplitudes.

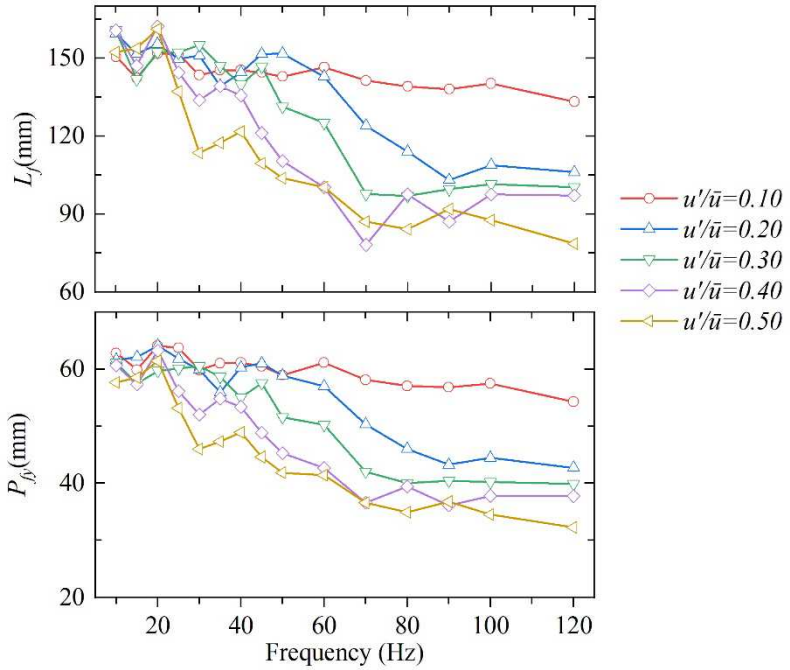


**Figure 4.** The time-averaged flame length ($L_f$) and height of the COM ($P_{fy}$) with different excitation frequencies and amplitudes.

Preprints (www.preprints.org) | NOT PEER-REVIEWED | Posted: 26 April 2023 doi:10.20944/preprints202304.0962.v1



The $St_f$ based on the flame length and the regenerated FDF with $St_f$ are shown in Figure 6. The range of $St_f$ is from 0.43 to 4.76. With low frequency excitation, the $St_f$ increases linearly with the excitation frequency. As the trend shows that the $L_f$ decreases much more at relatively high frequency and larger excitation amplitudes, the increasing slope of $St_f$ decreases with the increasing excitation amplitudes. The $St_f$ corresponding to the maximum gain is smaller than 0.50. When $St_f$ >3, the gain value is consistently below 0.25. The $St_f$ corresponding to the first local peak and valley of the gain are around 0.7-0.9 and 1.2-1.5, respectively. The $St_f$ range, which corresponds to the local peak and valley of the gain, is consistent with Szedlmayer et al.'s [48] results on a premixed flame. However, the control mechanism remains unclear. In the scenario where the acoustic eigenfrequency of the system is known, the $St_f$ can be utilized as a design parameter to ensure optimal deviation from the interval associated with higher gains.

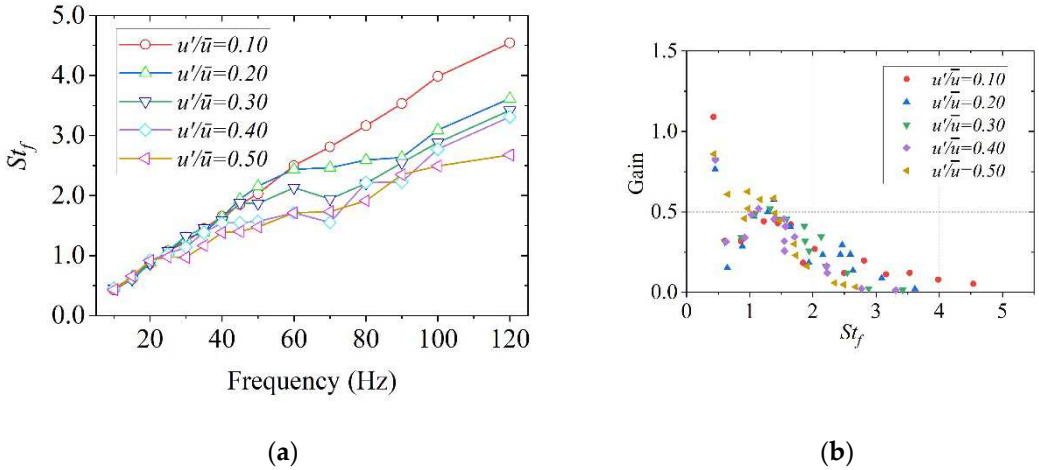


**Figure 5.** The calculated $St_f$ and the generated FDF: (a) The evolution of the $st_f$ with the excitation frequency; (b) The generated gain of the FDF with $St_f$.

*4.3 Comparison of Time Delay and Convection Time*

Experimental tests yielded the phase-lag, from which the time delay ($\tau_d$) of HRR and velocity fluctuations can be calculated in combination with the excitation frequency ($\tau_d=\Delta\varphi/(2\pi f)$). It is commonly believed that the disturbance induced by the acoustic excitation propagates along the flame at convective velocity [27]. Based on the jet velocity of air at the nozzle ($u_{cv}=u_0=3.52m/s$) and $P_{fy}$, the convective time ($\tau_{cv}$) can be calculated ($\tau_{cv}=P_{fy}/u_{cv}$). Figure 7 shows the comparison between the two parameters under different excitation frequencies and amplitudes. Anomalous values can be observed in the time delay under low-amplitude excitation at 20Hz, and significant delay is observed in these conditions. Under other conditions, it can be observed that the time delay rapidly decreases with increasing frequency in the low frequency range, and after the excitation frequency exceeds 20Hz, it remains relatively constant at around 0.01s. Moreover, after the frequency exceeds 20Hz, under different amplitude excitations, the delay time also remains around 0.01s and is not sensitive to changes in the excitation amplitude. The results of convective time ($\tau_{cv}$) and time delay ($\tau_d$) are consistent under high frequency and high amplitude excitation, whereas under other conditions there is deviation between the two. The distribution range of convective time in the 0.01-0.02s interval is generally consistent with that of time delay. Deviation mainly occurs under low frequency and low amplitude excitation conditions. In this operating range, the relatively long flame length may lead to inconsistencies between the height of the flame COM and the actual main oscillation zone of the flame. Additionally, the $u_{cv}$ may vary under different flame length. These two factors could potentially result in the deviation. Under high amplitude and high frequency, the flame is relatively short, and the deviation between the flame COM and the actual main oscillation zone of the flame is small, resulting in smaller deviations between the two. This problem deserves further research.

Preprints (www.preprints.org) | NOT PEER-REVIEWED | Posted: 26 April 2023 doi:10.20944/preprints202304.0962.v1



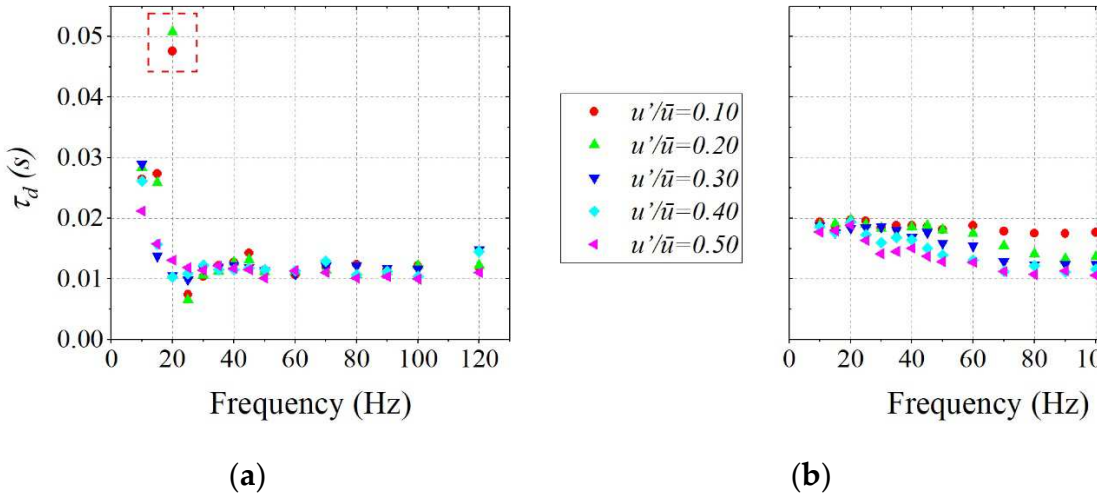


(a) (b)

**Figure 6.** The comparison of time delay and convection time under different excitation frequencies and amplitude: (a) the time delay calculated through the phase-lag; (b) the convection time calculated through the height of the COM and the constant convective velocity ($u_{cv}$=3.52m/s).

*4.4 The Dynamics of Flame Response*

In this section, we processed a sequence of CH* chemiluminescence and schlieren images to reveal the interaction mechanism between flow and reaction. We analyzed the heat release response at four excitation frequencies: 10Hz, 20Hz, 30Hz, and 100Hz for $u'/\bar{u}$=0.10 and 0.50. It is worth noting that the 10Hz case corresponds to the maximum gain of the FDF, whereas the 20Hz and 30Hz cases correspond to the local gain valley and peak, respectively. We also analyzed the response under relatively high-frequency excitations of 100Hz. The instantaneous CH* chemiluminescence images and the corresponding schlieren images under excitation amplitudes of 0.10 and 0.50 are shown in Figures 8–11. The phase angle of 0° corresponds to the maximum positive value of velocity fluctuation, while 180° corresponds to the minimum negative value of velocity fluctuation.

Under low-amplitude velocity excitation, flame height and overall phase remain relatively constant within an excitation cycle, particularly at high frequencies. Because of the short high-frequency excitation period, the HRR distribution only causes local lift and curling at the nozzle exit, without affecting the downstream flame region. Flame dynamic is mainly characterized by the changes in the wrinkle of the flame sheet, which can be observed more prominently from a side view. The number of wrinkles increases with increasing excitation frequency. High excitation amplitudes result in significant changes to flame morphology, with distinct differences in change characteristics depending on excitation frequency. At a low-frequency excitation of 10Hz, the flame undergoes multiple processes, including curling, bifurcation, overall extinguishment downstream, and gradual strengthening of the reaction upstream, as well as the formation of a vortex structure. In contrast, high-frequency excitation results in the formation of multiple distinct regions of heat release within a single cycle, with pronounced, vortex-like curling at their edges. Additionally, the main region of heat release increases in intensity from the nozzle and gradually decreases after reaching its maximum. The number of distinct regions of heat release increases as frequency increases. Specifically, a gradual transition between four layers of heat release regions was observed when excited frequency was 100Hz.

Preprints (www.preprints.org) | NOT PEER-REVIEWED | Posted: 26 April 2023 doi:10.20944/preprints202304.0962.v1



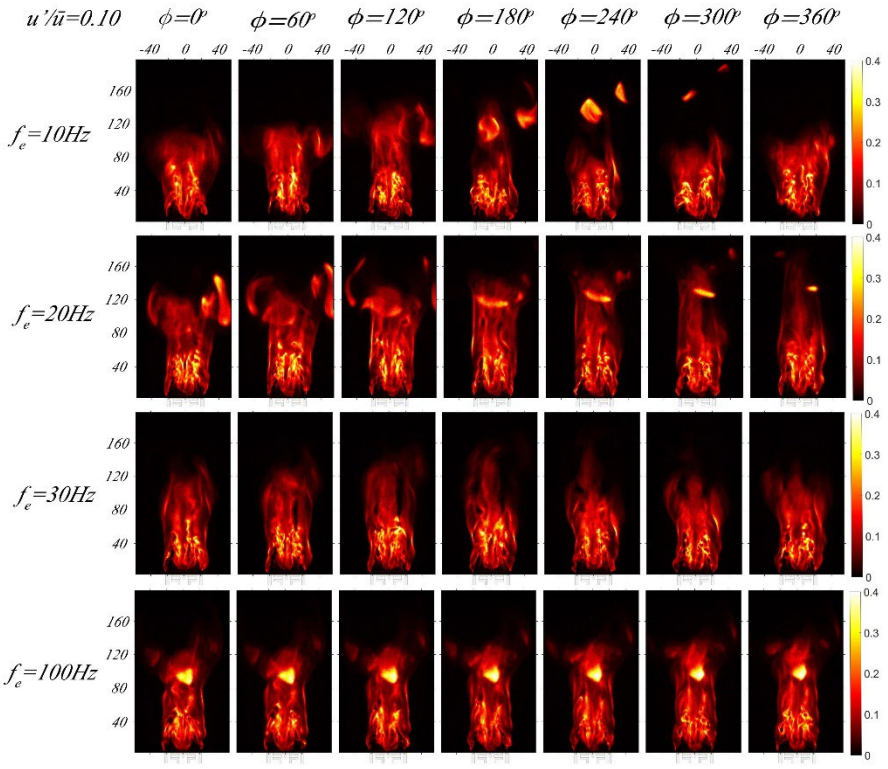


**Figure 7.** The instantaneous CH* chemiluminescence images in an excitation cycle at different excitation frequencies with $u'/\bar{u}$=0.10.

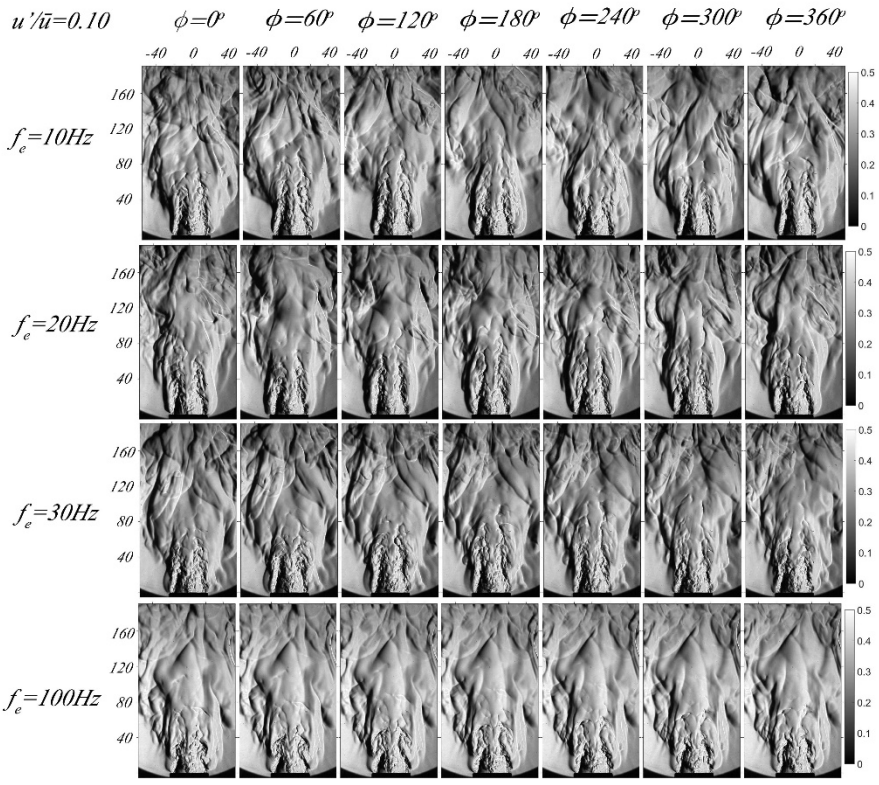


**Figure 8.** The instantaneous schlieren images in an excitation cycle at different excitation frequencies with u′/ū=0.10.

Preprints (www.preprints.org) | NOT PEER-REVIEWED | Posted: 26 April 2023 doi:10.20944/preprints202304.0962.v1



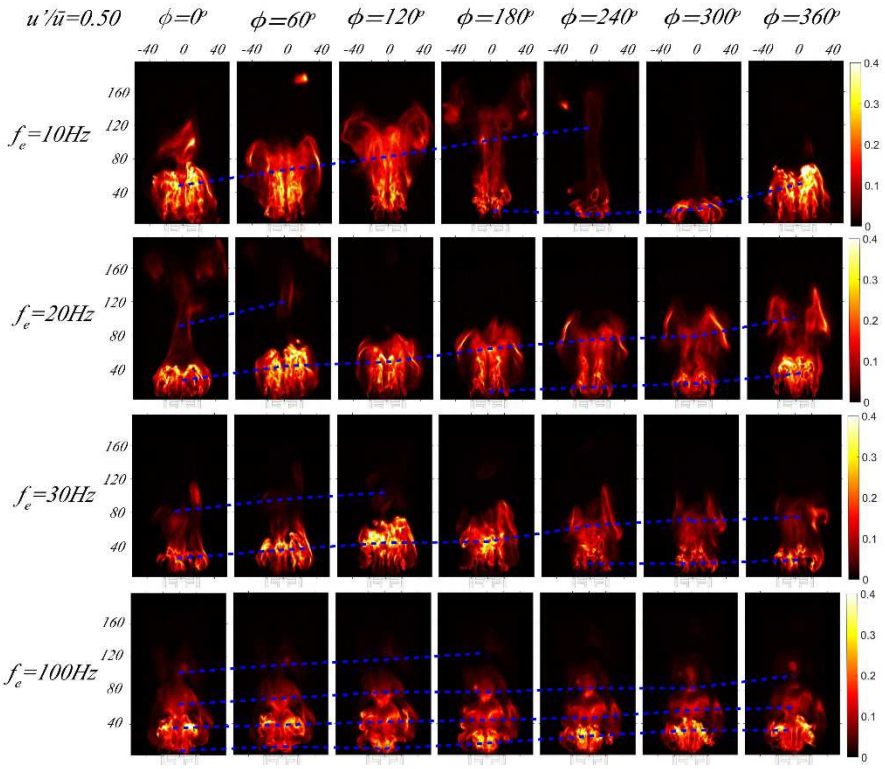


**Figure 9.** The instantaneous CH* chemiluminescence images in an excitation cycle at different excitation frequencies with $u'/\bar{u}$=0.50.

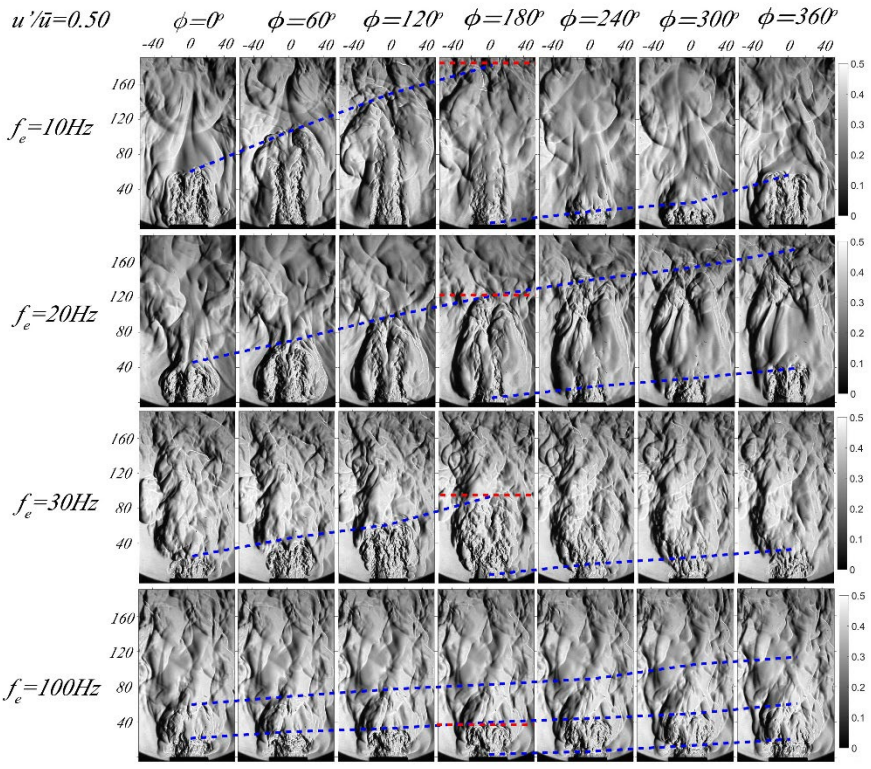


**Figure 10.** The instantaneous schlieren images of in an excitation cycle at different excitation frequencies with u′/ū=0.50.

Preprints (www.preprints.org) | NOT PEER-REVIEWED | Posted: 26 April 2023 doi:10.20944/preprints202304.0962.v1



A clearly observable propagation process of large vortex structures induced by flow perturbation can be seen in the instantaneous schlieren images. The convective velocity of the disturbance mentioned earlier can be analyzed through schlieren images. The minimum excitation velocity corresponds to the phase of 180 degrees, which is also the origin of vortex structure formation. The height at which perturbations propagate downstream over a single excitation period is defined as the convective wavelength $\lambda_f$ [50]. The convective wavelengths at different excitation frequencies and a fixed excitation amplitude of 0.5 are identified in Figure 11 with red lines. Meanwhile, the process of variation in the height of the large vortical structures is indicated with a green dashed line. The convective velocity of perturbations $u_{cf}$ can be calculated using the corresponding excitation frequency period $\tau_e$ and convective wavelength ($u_{cf}=\lambda_f/\tau_e$). The physical meaning of the ratio of flame length to convective wavelength ($L_f/\lambda_f$) is equivalent to the previously defined $St_f$. Hence, these two parameters were compared. The calculated convective wavelengths $\lambda_f$, convective velocity $u_{cf}$ and $L_f/\lambda_f$ for the four excitation frequencies are presented in Table 2. The results demonstrate an increase in convective velocity with increasing excitation frequency. The convective velocity is smaller than the jet velocity of 3.52m/s with lower frequency excitation, and relatively higher frequency excitation results in a convective velocity close to the jet velocity. This variation may be linked to the flame length under different excitation frequencies. Specifically, under low-frequency forcing, the flame length exhibits a longer extent while the convective velocity experiences a decrease downstream of the flame. This convective velocity attenuation behavior has also been observed in premixed flames, as reported in references [46,51]. Consequently, such a variation of $u_{cf}$ causes significant deviations in $L_f/\lambda_f$ and $St_f$ at low-frequency conditions. Therefore, when analyzing the relationship between flame response and $St_f$, it is necessary to consider the changes in convective velocity.

**Table 1.** The calculated parameters related to convective velocity $u_{cf}$.

| $f_e$(Hz) | 10 | 20 | 30 | 100 |
|---|---|---|---|---|
| $\lambda_f$ (mm) | 190.4 | 121.7 | 87.6 | 30.9 |
| $\tau_e$ (s) | 0.100 | 0.050 | 0.033 | 0.010 |
| $L_f$ (mm) | 152.4 | 161.2 | 113.6 | 87.6 |
| $u_{cf}$ (m/s) | 1.90 | 2.43 | 2.63 | 3.61 |
| $L_f/\lambda_f$ | 0.80 | 1.32 | 1.29 | 2.42 |
| $St_f$ | 0.43 | 0.92 | 0.97 | 2.43 |

*4.5 Axial Distribution of Heat Release Oscillation*

The axial distribution of heat release oscillations for various excitation frequencies is shown in Figure 12 at a velocity excitation amplitude of 0.50. Notably, distinct axial oscillation distributions are present across the different excitation frequencies. At a low frequency of 10Hz, the velocity excitation predominantly causes positive heat release oscillations in the upstream within the 0°-180° phase range. Additionally, the positive oscillation region progressively diminishes and propagates downstream. Following the 180-degree phase, when the excitation velocity reaches its minimum negative value, the entire middle and lower region begin to experience flameout. This results in a negative oscillation of heat release. Eventually, with the increase of velocity fluctuation, the heat release in the upstream region increases, inducing positive oscillation and entering the next cycle. At 10Hz excitation, positive or negative oscillations dominantly appear in the axial distribution of heat release, and the oscillation zones are relatively broad. Subsequently, the corresponding oscillation amplitude is also significant, and this behavior is associated with $St_f$<1. This oscillation form reveals the primary reason for the large gain of the flame under low-frequency (10Hz) excitation.

Under 20Hz excitation, unlike 10Hz, the positive and negative oscillation zones coexist at various phases. Furthermore, the amplitudes of these two zones are equal, leading to a relatively small total heat release fluctuation value. As a result, this is the main reason for the appearance of the gain valley around 20Hz. Under 30Hz excitation, there are two opposing oscillation regions, but their relative relationship is significantly different with 20Hz excitation frequency. Specifically, regarding

Preprints (www.preprints.org) | NOT PEER-REVIEWED | Posted: 26 April 2023 doi:10.20944/preprints202304.0962.v1



the middle forward oscillation region, the corresponding region for 30Hz excitation reaches its maximum value at $\phi$=120° and then quickly decays, which causes single-region predominance for most phases. This feature, similar to that seen under 10Hz excitation, leads to the appearance of local gain peaks under 30Hz excitation. Under 100Hz high-frequency excitation, multiple alternating oscillation regions appear. At different phase angles, the heat release oscillations have a wavenumber ranging from 2.0 to 2.5 within the flame length ($L_f$=87.6mm). This is consistent with the $St_f$ (2.43) and the number of heat release layers (2-3) in Figure 10. Additionally, the oscillation amplitude of the downstream region decreases significantly relative to the upstream region. This multi-region alternating structure under high-frequency excitation means that positive and negative oscillations at the same moment have a counteractive effect, and the dispersed oscillation amplitude is relatively small, which leads to a relatively low gain under high-frequency excitation. This is the main reason for the low-pass filtering characteristic of the flame.

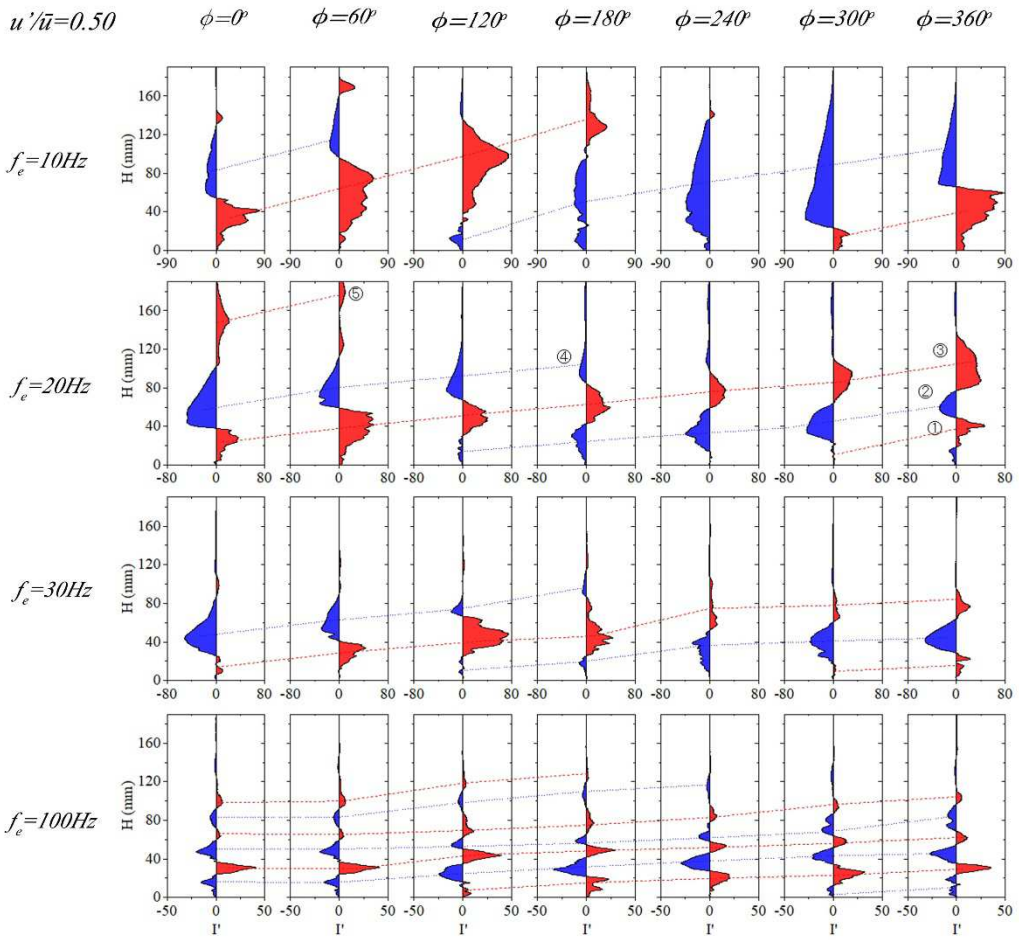


**Figure 11.** The axial distribution of heat release oscillations with variation of phase angles at different excitation frequencies and $u'/\bar{u}$=0.10.

The phase-lag varies significantly at different excitation amplitudes at 20Hz, presenting another noteworthy phenomenon. Therefore, we analyzed the axial distribution of heat release oscillation under the condition of 20Hz and 0.1 excitation amplitude, as shown in Figure 13. By comparing, we found that, although the number of axial regions is consistent under two different amplitudes, the variation trends of the five oscillation regions differ significantly, especially in the phase range of $\phi$= 0~180°. The overall HRR oscillation and the normalized velocity fluctuation with different phase angles under excitation amplitudes of 0.1 and 0.5 are presented in Figure 14. Under a low-amplitude excitation (u'/ū=0.10), the positive oscillation of the region number 5 decreased noticeably while the negative oscillation of region number 4 remained unchanged. As a result, there was a diminishing

Preprints (www.preprints.org) | NOT PEER-REVIEWED | Posted: 26 April 2023 doi:10.20944/preprints202304.0962.v1



trend in HRR during phase interval of 0~120°. Following the 120° phase, a decline in negative oscillation of region number 4 was observed while positive oscillation of region number 3 intensified, leading to an early rise in HRR compared to the phase of velocity fluctuations. In contrast, when the excitation amplitude was high at 0.5, both of the positive oscillation of region number 4 and the negative oscillation of region number 5 experienced attenuation. Meanwhile, the positive oscillation of region number 3 increased initially, decreased subsequently, and dominated in value after the 60° phase. As a result, the overall HRR first increased, then decreased within the phase range of 0 to 120°. After the 120° phase, the negative oscillation of region number 2 emerged and gradually intensified, causing a continued decrease in overall HRR until a phase angle of 300° was reached. At a phase angle of 360°, an increase in HRR was observed due to an increase in the positive oscillation of region number 3. Consequently, there was a delay of approximately 90° between the lowest HRR and the smallest value of velocity fluctuation.

The relative change trend of the oscillation region varies depending on different excitation amplitudes, resulting in a considerable phase difference. This shift is primarily due to the proximity of the positive and negative oscillation amplitude, causing the overall HRR to be more sensitive to variations within a single oscillation region. These conditions are susceptible to changes of the excitation frequency or amplitude, leading to considerable phase shifts.

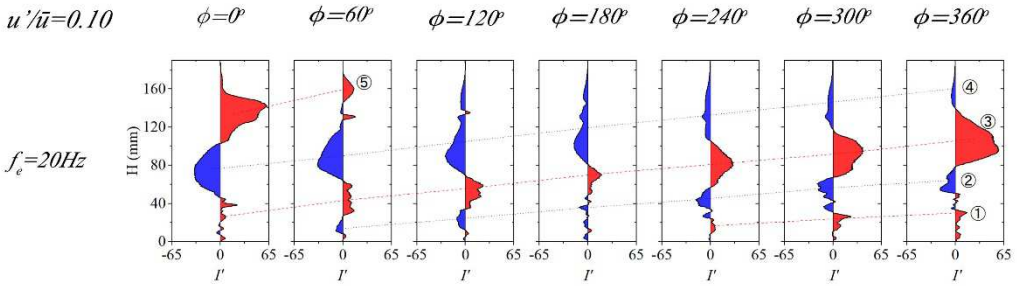


**Figure 12.** The axial distribution of heat release oscillation with variation of phase angles at $f_e$=20 and $u'/\bar{u}$=0.10.

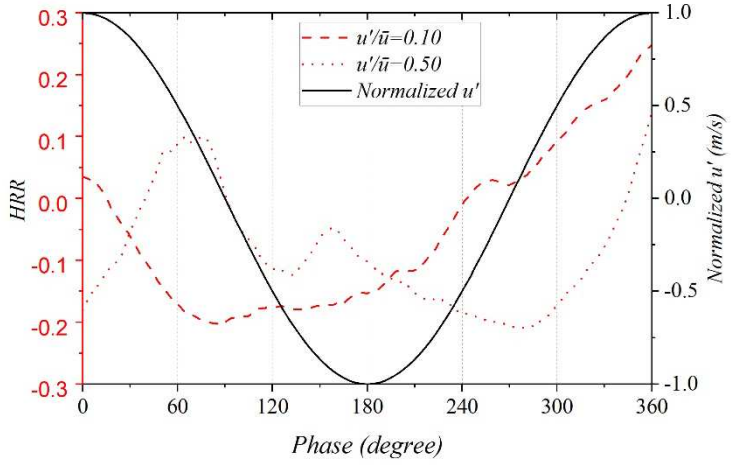


**Figure 13.** The evolution of the HRR and the normalized velocity fluctuation with respect to the phase angle at two different excitation amplitudes, namely 0.10 and 0.50, at excitation frequency of 20Hz.

## 5 Conclusions

This study experimentally investigates the nonlinear heat release response of a non-premixed methane-air flame to low frequency acoustic excitations. The experiment measures the flame describing function (FDF) and analyzes the CH* chemiluminescence and schlieren images. It reveals

the governing mechanisms of the nonlinear response. The FDF is characterized by low-pass filtering. When $St_f$ >3, the gain value is consistently below 0.25. The highest gain is observed at $St_f$ = 0.43, and local valley and peak values of gain are observed at $St_f$ ranges of 0.7-0.9 and 1.2-1.5, respectively. The local gain peaks and valleys of the FDF are related to the spatial distribution wavenumber of the heat release at different $St_f$. As $St_f$ increases, the oscillation zone of the flame shifts to higher wavenumbers, and the relative intensity of the positive and negative oscillation zones result in different cancellation effects. When the positive and negative oscillation zones are close to each other, the cancellation effect is at its maximum, leading to the minimum gain. In this condition, variations in frequency or amplitude can cause anomalous changes in the phase-lag of the flame, as the overall HRR becomes more sensitive to changes in a certain oscillation zone. Under relatively high-frequency excitation conditions, multiple oscillation zones of heat release along the flame are observed. The dispersion of multiple oscillation zones, as well as the cancellation effect of oscillation zones, are the primary causes of the low-pass filtering characteristic of the flame. The flame length significantly decreases under large amplitude and high frequency excitation. Specifically, the normalized flame length ($L_f/D$) decreases from 3.79 to 2.37 as the excitation amplitude increases at an excitation frequency of 100Hz. The delay time corresponding to the phase-lag exhibits the same with the convection time of disturbances under conditions of large-amplitude and high-frequency excitation. This behavior may be related to the accuracy determination of the average convective velocity and the consistency of the oscillation region and the COM of flame with short flame. These findings may provide insights into the stable design of non-premixed flame related to thermoacoustic instability.

**Author Contributions:** Conceptualization, Tong Zhu. and Deng Pan.; methodology, Chenzhen Ji.; investigation, Deng Pan; resources, Tong Zhu; data curation, Deng Pan; writing—original draft preparation, Deng Pan; writing—review and editing, Deng Pan and Chenzhen Ji; visualization, Deng Pan; supervision, Tong Zhu; funding acquisition, Tong Zhu. All authors have read and agreed to the published version of the manuscript.

**Funding:** This research was funded by National Natural Science Foundation of China, grant number 51976140, and Science and Technology Commission of Shanghai Municipality, grant number 20DZ1204902.

**Conflicts of Interest:** The authors declare no conflict of interest.

## References

1. Acharya, V.S.; Bothien, M.R.; Lieuwen, T.C. Non-Linear Dynamics of Thermoacoustic Eigen-Mode Interactions. *Combust. Flame* **2018**, *194*, 309–321.
2. Shreekrishna; Hemchandra, S.; Lieuwen, T. Premixed Flame Response to Equivalence Ratio Perturbations. *Combust. Theory Model.* **2010**, 14, 681–714.
3. O'Connor, J.; Vanatta, C.; Mannino, J.; Lieuwen, T. Mechanisms for Flame Response in a Transversely Forced Flame. In Proceedings of the 7th US national technical meeting of the combustion institute, Atlanta, USA, 20-23 March **2011**.
4. Preetham, S.H.; Lieuwen, T.C. Response of Turbulent Premixed Flames to Harmonic Acoustic Forcing. *Proc. Combust. Inst.* **2007**, 31, 1427–1434.
5. Durox, D. Theoretical and Experimental Determinations of the Transfer Function of a Laminar Premixed Flame. *Proc. Combust. Inst.* **2000**, *28*, 765–773.
6. Fleifil, M.; Annaswamy, A.M.; Ghoneim, Z.A.; Ghoniem, A.F. Response of a Laminar Premixed Flame to Flow Oscillations: A Kinematic Model and Thermoacoustic Instability Results. *Combust. Flame* **1996**, *106*, 487–510.
7. Merk, M.; Gaudron, R.; Silva, C.; Gatti, M.; Mirat, C.; Schuller, T.; Polifke, W. Prediction of Combustion Noise of an Enclosed Flame by Simultaneous Identification of Noise Source and Flame Dynamics. *Proc. Combust. Inst.* **2019**, *37*, 5263–5270.
8. Boudy, F.; Schuller, T.; Durox, D.; Candel, S. The Flame Describing Function (FDF) Unified Framework for Combustion Instability Analysis: Progress and Limitations. In Proceedings of International Workshop on Non-normal and Nonlinear effects in aero- and thermo-acoustics, Munich, German, 18-21 June **2013**.
9. Dowling, A.P. Nonlinear Self-Excited Oscillations of a Ducted Flame. *J. Fluid Mech.* **1997**, *346*, 271–290.
10. Noiray, N.; Durox, D.; Schuller, T.; Candel, S. A Unified Framework for Nonlinear Combustion Instability Analysis Based on the Flame Describing Function. *J. Fluid Mech.* **2008**, *615*, 139–167.
11. Krediet, H.J.; Beck, C.H.; Krebs, W.; Schimek, S.; Paschereit, C.O.; Kok, J.B.W. Identification of the Flame Describing Function of a Premixed Swirl Flame from LES. *Combust. Sci. Technol.* **2012**, *184*, 888–900.
12. Tay-Wo-Chong, L.; Bomberg, S.; Ulhaq, A.; Komarek, T.; Polifke, W. Comparative Validation Study on Identification of Premixed Flame Transfer Function. *J. Eng. Gas Turbines Power* **2012**, *134*, 1–8.

13. Kim, K.T.; Lee, H.J.; Lee, J.G.; Quay, B.D.; Santavicca, D. Flame Transfer Function Measurement and Instability Frequency Prediction Using a Thermoacoustic Model. In Proceedings of the ASME Turbo Expo, Orlando, USA, 8-12 June **2009**.
14. Alemela, P.R.; Fanca, D.; Ettner, F.; Hirsch, C.; Sattelmayer, T.; Schuermans, B. Flame Transfer Matrices of a Premixed Flame and a Global Check with Modelling and Experiments. In Proceedings of the ASME Turbo Expo; Berlin, Germany, 9-13 June **2008**.
15. Gaudron, R.; Gatti, M.; Mirat, C.; Schuller, T. Impact of the Injector Size on the Transfer Functions of Premixed Laminar Conical Flames. *Combust. Flame* **2017**, *179*, 138–153.
16. Schuller, T.; Durox, D.; Candel, S. A Unified Model for the Prediction of Laminar Flame Transfer Functions: Comparisons between Conical and V-Flame Dynamics. *Combust. Flame* **2003**, *134*, 21–34.
17. Boudy, F.; Durox, D.; Schuller, T.; Candel, S. Nonlinear Mode Triggering in a Multiple Flame Combustor. *Proc. Combust. Inst.* **2011**, *33*, 1121–1128.
18. Hermeth, S.; Staffelbach, G.; Gicquel, L.Y.M.; Anisimov, V.; Cirigliano, C.; Poinsot, T. Bistable Swirled Flames and Influence on Flame Transfer Functions. *Combust. Flame* **2014**, *161*, 184–196.
19. Ćosić, B.; Terhaar, S.; Moeck, J.P.; Paschereit, C.O. Response of a Swirl-Stabilized Flame to Simultaneous Perturbations in Equivalence Ratio and Velocity at High Oscillation Amplitudes. *Combust. Flame* **2015**, *162*, 1046–1062.
20. Palies, P.; Durox, D.; Schuller, T.; Candel, S. Experimental Study on the Effect of Swirler Geometry and Swirl Number on Flame Describing Functions. *Combust. Sci. Technol.* **2011**, *183*, 704–717.
21. Shanbhogue, S.; Shin, D.; Hemchandra, S.; Plaks, D.; Lieuwen, T. Flame Sheet Dynamics of Bluff-Body Stabilized Flames during Longitudinal Acoustic Forcing. *Proc. Combust. Inst.* **2009**, *32*, 1787–1794.
22. Schuermans, B.; Bellucci, V.; Flohr, P.; Paschereit, C.O. Thermoacoustic Flame Transfer Function of a Gas Turbine Burner in Premix and Pre- Premix Combustion. In Proceedings of the AIAA Aerospace Sciences Meeting and Exhibit, Reno, USA, 5-8 January, **2004**.
23. Kim, K.T.; Santavicca, D.A. Generalization of Turbulent Swirl Flame Transfer Functions in Gas Turbine Combustors. *Combust. Sci. Technol.* **2013**, *185*, 999–1015.
24. Kim, K.T.; Lee, J.G.; Quay, B.D.; Santavicca, D.A. Spatially Distributed Flame Transfer Functions for Predicting Combustion Dynamics in Lean Premixed Gas Turbine Combustors. *Combust. Flame* **2010**, *157*, 1718–1730.
25. Tyagi, M.; Chakravarthy, S.R.; Sujith, R.I. Unsteady Combustion Response of a Ducted Non-Premixed Flame and Acoustic Coupling. *Combust. Theory Model.* **2007**, *11*, 205–226.
26. Chandrasekhar, S. V.; Chakravarthy, S.R. Response of Non-Premixed Ducted Flame to Transverse Oscillations and Longitudinal Acoustic Coupling. In Proceedings of the 43rd AIAA/ASME/SAE/ASEE Joint Propulsion Conference, Cincinnati, USA, 8-11, July, **2007**.
27. Magina, N.; Acharya, V.; Lieuwen, T. Forced Response of Laminar Non-Premixed Jet Flames. *Prog. Energy Combust. Sci.* **2019**, *70*, 89–118.
28. Magina, N.; Shin, D.H.; Acharya, V.; Lieuwen, T. Response of Non-Premixed Flames to Bulk Flow Perturbations. *Proc. Combust. Inst.* **2013**, *34*, 963–971.
29. Tim C.Lieuwen. *Unsteady Combustor Physics*, 1st ed.; Cambridge University Press: New York, USA, 2012; pp. 364-369.
30. Yao, Z.; Zhu, M. A Distributed Transfer Function for Non-Premixed Combustion Oscillations. *Combust. Sci. Technol.* **2012**, *184*, 767–790.
31. Jiang, J.; Jing, L.; Zhu, M.; Jiang, X. A Comparative Study of Instabilities in Forced Reacting Plumes of Nonpremixed Flames. *J. Energy Inst.* **2016**, *89*, 456–467.
32. Farhat, S.; Kleiner, D.; Zhang, Y. Jet Diffusion Flame Characteristics in a Loudspeaker-Induced Standing Wave. *Combust. Flame* **2005**, *142*, 317–323.
33. Farhat, S.A.; Ng, W.B.; Zhang, Y. Chemiluminescent Emission Measurement of a Diffusion Flame Jet in a Loudspeaker Induced Standing Wave. *Fuel* **2005**, *84*, 1760–1767.
34. Chen, L.W.; Wang, Q.; Zhang, Y. Flow Characterisation of Diffusion Flame in a Standing Wave. *Exp. Therm. Fluid Sci.* **2012**, *41*, 84–93.
35. Chen, L.W.; Wang, Q.; Zhang, Y. Flow Characterisation of Diffusion Flame under Non-Resonant Acoustic Excitation. *Exp. Therm. Fluid Sci.* **2013**, *45*, 227–233.
36. Sun, Y.; Zhao, D.; Ni, S.; David, T.; Zhang, Y. Entropy and Flame Transfer Function Analysis of a Hydrogen-Fueled Diffusion Flame in a Longitudinal Combustor. *Energy* **2020**, *194*, 116870.
37. Kim, T.; Ahn, M.; Lim, D.; Yoon, Y. Flame Describing Function and Combustion Instability Analysis of Non-Premixed Coaxial Jet Flames. *Exp. Therm. Fluid Sci.* **2022**, *136*, 110642.
38. Fu, X.; Yang, F.; Guo, Z. Combustion Instability of Pilot Flame in a Pilot Bluff Body Stabilized Combustor. *Chinese J. Aeronaut.* **2015**, *28*, 1606–1615.
39. Ahn, B.; Lee, J.; Jung, S.; Kim, K.T. Low-Frequency Combustion Instabilities of an Airblast Swirl Injector in a Liquid-Fuel Combustor. *Combust. Flame* **2018**, *196*, 424–438.

40. Chen, Y.C.; Chang, C.C.; Pan, K.L.; Yang, J.T. Flame Lift-off and Stabilization Mechanisms of Nonpremixed Jet Flames on a Bluff-Body Burner. *Combust. Flame* **1998**, *115*, 51–65.
41. Hardalupas, Y.; Selbach, A. Imposed Oscillations and Non-Premixed Flames. *Prog. Energy Combust. Sci.* 2002, *28*, 75–104.
42. Putnam, A.A. Combustion Roar as Observed in Industrial Furnaces. *J. Eng. Power* **1982**, *104*, 867–873.
43. Putnam, A.; Faulkner, L. An Overview of Combustion Noise. *J. Energy* **1983**, *7*, 458–469.
44. Chung, J.Y.; Blaser, D.A. Transfer Function Method of Measuring In-Duct Acoustic Properties. I. Theory. *J. Acoust. Soc. Am.* **1980**, *68*, 907–913.
45. Balachandran, R.; Ayoola, B.O.; Kaminski, C.F.; Dowling, A.P.; Mastorakos, E. Experimental Investigation of the Nonlinear Response of Turbulent Premixed Flames to Imposed Inlet Velocity Oscillations. *Combust. Flame* **2005**, *143*, 37–55.
46. Kim, D.; Lee, J.G.; Quay, B.D.; Santavicca, D.A.; Kim, K.; Srinivasan, S. Effect of Flame Structure on the Flame Transfer Function in a Premixed Gas Turbine Combustor. *J. Eng. Gas Turbines Power* **2010**, *132*, 1–7.
47. Ranalli, J.A.; Ferguson, D.; Martin, C. Simple Analysis of Flame Dynamics via Flexible Convected Disturbance Models. *J. Propuls. Power* **2012**, *28*, 1268–1276.
48. Szedlmayer, M.T.; Quay, B.D.; Samarasinghe, J.; De Rosa, A.; Lee, J.G.; Santavicca, D.A. Forced Flame Response of a Lean Premixed Multi-Nozzle Can Combustor. In Proceedings of the ASME Turbo Expo, Vancouver, Canada, 6-10 June **2011**.
49. Jones, B.; Lee, J.G.; Quay, B.D.; Santavicca, D.A. Flame Response Mechanisms Due to Velocity Perturbations in a Lean Premixed Gas Turbine Combustor. *J. Eng. Gas Turbines Power* **2011**, *133*, 1–9.
50. Shin, D.H.; Lieuwen, T. Flame Wrinkle Destruction Processes in Harmonically Forced, Turbulent Premixed Flames. *J. Fluid Mech.* **2013**, *721*, 484–513.
51. Liu, W.; Xue, R.; Zhang, L.; Yang, Q.; Wang, H. Nonlinear Response of a Premixed Low-Swirl Flame to Acoustic Excitation with Large Amplitude. *Combust. Flame* **2022**, *235*, 111733.